REDETERMINATION OF ZERO-FIELD SPLITTING IN $[Co(qu)_2Br_2]$ AND $[Ni(PPh_3)_2Cl_2]$ COMPLEXES

DOMINIK LOMJANSKÝ[1], FILIP VARGA[1], CYRIL RAJNÁK[1], JÁN MONCOĽ[2], ROMAN BOČA[1], JÁN TITIŠ[1]

[1] *Department of Chemistry, Faculty of Natural Sciences, University of SS. Cyril and Methodius in Trnava, Nám. J. Herdu 2, Trnava, SK-917 01, Slovak Republic (lomjanskyd@gmail.com)*
[2] *Institute of Inorganic Chemistry, FCHPT, Slovak University of Technology, Bratislava, SK-812 37, Slovak Republic*

Abstract: A mononuclear Co^{II} complex, $[Co(qu)_2Br_2]$, and Ni^{II} complex, $[Ni(PPh_3)_2Cl_2]$, (*qu* = quinoline, PPh_3 = triphenylphosphine) have been reinvestigated. Their crystal and molecular structures are reported along with IR and UV-Vis spectra. Magnetism of both complexes has been studied by using the DC SQUID magnetometry. These complexes exhibit a moderate magnetic anisotropy expressed by zero-field splitting parameter *D*. The *D*-value is positive for both complexes with $D/hc = +5.94$ cm^{-1} and $D/hc = +12.76$ cm^{-1}, that is also confirmed by *ab initio* calculations.

Key words: tetracoordinate complexes, electronic spectra, magnetic susceptibility, magnetization, zero-field splitting

1. Introduction

Detection of static and dynamic magnetic properties of mononuclear 3d metal complexes is an important task in the emerging field of molecular magnetism. Single-molecule magnets (SMMs), as the main objects of interest, show slow magnetic relaxation as a consequence of the energy barrier ($E_b \approx |D|S^2$, where *D* is axial zero-field splitting (ZFS) parameter) for the magnetization reversal between the two lowest $M_S = \pm S$ states (GATTESCHI *et al.,* 2006; FROST *et al.,* 2016). SMMs are a major scientific target because of their potential applications in high-density magnetic memories and quantum-computing devices.

The zero-field splitting represents a fine structure of the electronic energy levels that appears as a result of the splitting of the crystal-field terms into crystal-field multiplets. It is characterized by the axial ZFS parameter *D* that is related to the energy gap between the ground and excited states (BOČA, 2004; BOČA, 2006). Despite the relatively wide range of knowledge, a rational design of the *D*-parameter is still far from the routine, though there is a need of this when tuning the properties of the SMMs. The sign of the *D*-parameter is either negative or positive and it adopts values between 10^{-2} – 10^{2} cm^{-1}. Some insights to this target brought the magnetostructural *D*-correlations that bring a linear relationship between the axial distortion of the octahedron and the *D*-parameter in a series of Ni^{II} hexacoordinate complexes (TITIŠ and BOČA, 2010). For hexacoordinate Co^{II} complexes the magnetostructural *D*-correlation has also been outlined (TITIŠ and BOČA, 2011).

DOI 10.1515/nbec-2016-0020

The case of tetracoordinate complexes is no less interesting. Tetrahedral ligand environments produce weaker crystal-fields in comparison with its octahedral counterparts. This results to the enhanced second-order perturbation (as a consequence of the spin-orbit coupling) of the ground crystal-field term, and thus to the significantly larger *D*-values (IDEŠICOVÁ *et al.,* 2013). The present communication compares magnetic behavior of two different systems, the tetracoordinate Co^{II} (Kramers ion, $S = 3/2$) and tetracoordinate Ni^{II} (non-Kramers ion, $S = 1$). Reinvestigation of complexes $[Co(qu)_2Br_2]$ and $[Ni(PPh_3)_2Cl_2]$ (*qu* = quinoline, PPh3 = triphenylphosphine), hereafter **1** and **2**, using the DC magnetometry and contemporary methods of quantum chemistry represents the aim of this study. In tetracoordinate Co^{II} complexes the ground term $^4A_2(T_d)$ is split into the ground and excited multiplets (each referring to a Kramers doublet) separated by 2*D*. In reference T_d symmetry the ground term of the Ni^{II} ion is the orbitally degenerate $^3T_2$. This term in lower symmetry (D_{2d}) is split into the ground $^3A_2$ and excited ^3E terms. Spin-orbit coupling further split the $^3A_2$ ground term into $M_S = 0$ and $M_S = \pm 1$ multiplets. Difference between them is equal to *D*.

2. Materials and Methods

2.1. Synthesis

The compound **1**, $[Co(qu)_2Br_2]$, has been prepared as follows. A solution of 0.218 g (1 mmol) $CoBr_2$ in 10 cm^3 of acetonitrile was added to the solution of 0.258 g (2 mmol) of *qu* in 10 cm^3 of acetonitrile under an intense stirring (the molar ratio *qu*:$CoBr_2$ = 2:1). A mixture was stirred for 3 h at room temperature. The filtrate was left for 3 days for a spontaneous evaporation. The dark blue crystals were separated on Büchner funel.

The compound **2**, $[Ni(PPh_3)_2Cl_2]$, has been prepared as follows. A solution of 0.238 g (1 mmol) of $NiCl_2{\cdot}6H_2O$ in 20 cm^3 of distilled water and 5 cm^3 of acetic acid was added. A solution of 0.525 g (2 mmol) of PPh_3 in 2.5 cm^3 of acetic acid was slowly added in solution of $NiCl_2{\cdot}6H_2O$ using a Pasteur pipette. Deep blue crystals were obtained after 20 hours standing.

2.2. Physical measurements

Elemental analysis was carried out on FlashEA 1112 (ThermoFinnigan). IR spectra were measured using the ATR method (Magna FTIR 750. Nicolet) in the 400 – 4 000 cm^{-1} region. Electronic spectra were measured in Nujol mull (Specord 200, Analytical Jena) in the range 9 000 – 50 000 cm^{-1}. Magnetic data were taken with the SQUID magnetometer (MPMS-XL7. Quantum Design) using the RSO mode of detection. The susceptibility data were scanned in the temperature range 2 – 300 K at the applied field of $B = 0.1$ T. The magnetization has been measured at $T = 2.0$ and 4.6 K. Raw data were corrected for the underlying diamagnetism using estimate of $\chi_{dia}/(10^{-12}\ m^3\ mol^{-1}) = -5M[g\ mol^{-1}]$.

2.3. Quantum-chemical calculations

Ab initio calculations were performed with ORCA 3.0.3 computational package at the experimental geometry determined by the X-ray diffraction for the mononuclear entity (NEESE 2012). Relativistic effects were included in the calculations by zero order regular approximation (ZORA) together with the scalar relativistic contracted version of TZVP basis functions. The calculations of ZFS parameters were based on state average complete active space self-consistent field (SA-CASSCF) wave functions complemented by NEVPT2 theory (ANGELI *et al.,* 2001; ANGELI *et al.,* 2002; ANGELI *et al.,* 2004; ATANASOV *et al.,* 2011). The calculations utilized the RI approximation with appropriate decontracted auxiliary basis set and the RIJCOSX approximation to exact exchange. Increased integration grids (Grid4) and tight SCF convergence criteria were used. The ZFS parameters were calculated through quasi-degenerate perturbation theory (QDPT) in which an approximation to the Breit-Pauli form of the spin-orbit coupling operator (SOMF) and the effective Hamiltonian theory was utilized (NEESE, 2005; GANYUSHIN and NEESE, 2006; NEESE, 2007).

Table 1. Selected crystal data.

Compound	**1**, $[Co(qu)_2Br_2]$	**2**, $[Ni(PPh_3)_2Cl_2]$
Chemical formula	$C_{18}H_{14}Br_2CoN_2$	$C_{36}H_{30}Cl_2NiP_2$
M(g mol^{-1})	477.06	654.15
Crystal system	Triclinic	monoclinic
Space group	P -1	$P2_1/c$
T (K)	293(2)	298(2)
a (Å)	8.685(4)	11.620(4)
b (Å)	9.637(5)	8.202(2)
c (Å)	11.232(5)	17.387(7)
α (°)	80.671(4)	90
β (°)	74.592(4)	107.009(4)
γ (°)	73.296(4)	90
V (Å^3)	864.45(8)	1583.80(10)
Z	2	2
Radiation type	Mo Kα (λ=0.71073)	Mo Kα (λ=0.71073)
μ (mm^{-1})	5.614	0.907
F(000)	466	676
Index ranges	-11≤h≤11,-12≤k≤12, -14≤l≤14	-8≤h≤14,-10≤k≤10, -21≤l≤19
ρ calc.(g cm^{-3})	1.833	1.372
Final R indexes [$F2 > 2\sigma(F2)$], $wR_2(F2)$	R_1=0.0321 wR_2=0.0738	R_1=0.0322 wR_2=0.0742
R indices (all data)	R_1=0.0453 wR_2=0.0804	R_1=0.0453 wR_2=0.0812
Data / restrains / parameters	3814/0/208	3232/0/186
Goodness of fit	1.029	1.033

2.4. X-ray crystallography

Data collection and cell refinement were carried out using a κ-axis diffractometer Gemini R CCD (OXFORD DIFFRACTION, 2010) with graphite monochromated Mo Kα radiation. The diffraction intensities were corrected for Lorentz and polarization factors. The structures were solved by direct methods using SIR-97 (ALTOMARE, 1999) or SHELXS-97 (SHELDRICK, 2008) and refined by the full-matrix least-squares procedure with SHELXL-97 (CLARK, 1995). The analytical or multi-scan absorption corrections were made by using CRYSALIS-RED (Oxford Diffraction 2010). Geometrical analyses were performed with SHELXL-97. Crystal data and conditions of data collection and refinement are reported in Table 1.

3. Results and Discussion

The molecular structures with thermal ellipsoids of **1** and **2** are presented in Fig. 1. The coordination environment of **1** consists of two donor nitrogen atoms of two quinoline ligands completed by two bromide anions. The coordination sphere of **2** consists of two donor phosphorus atoms of triphenylphospine ligands completed by two chloride anions. In both cases the chromophore, $\{CoN_2Br_2\}$ and $\{CoP_2Cl_2\}$, refers to a distorted tetrahedron. Important structural parameters, metal-ligand bond distances and bond angles, for the studied complexes are collected in Table 2.

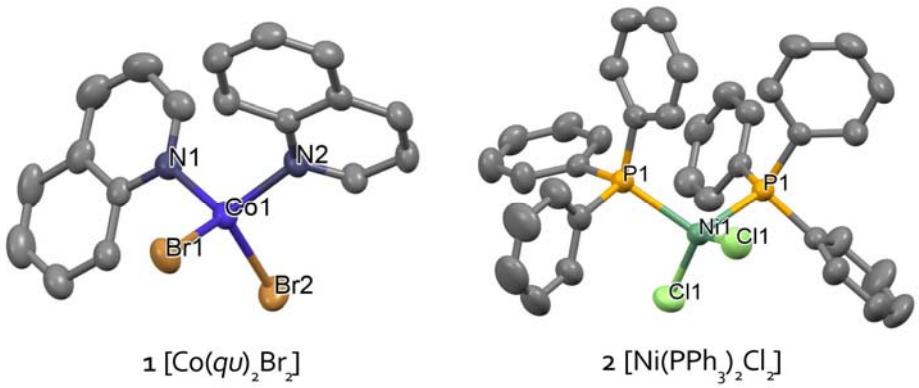

Fig. 1. Molecular structure of complexes **1** and **2** (thermal ellipsoids shown at 50 % of probability level, hydrogens omitted for clarity).

We note that compounds under study have already been structurally characterized and are deposited in structural database (CCDC, 2016) under refcodes TUSQAB (KORCHAGIN *et al.,* 2015) and CLTPNI (GARTON *et al.,* 1963). By comparing the structural characteristics of these structures with complexes studied in this work we note marked similarities especially for the Co^{II} complex. For the Ni^{II} complex the differences are more pronounced. One can found a shorter Ni-P distances (2.277 Å) and longer Ni-Cl distances (2.274 Å) in the CLTPNI structure.

Furthermore, the bond angles in CLTPNI (P-Ni-P, 116.6° and Cl-Ni-Cl, 123.2°) also shown significant deviations from those in **2**.

Table 2. Selected bond lengths (Å) and angles (°) in **1** and **2**.

	bond lengths	angles
1, $[Co(qu)_2Br_2]$	Co(1)-Br(1) 2.377(5)	Br(1)-Co(1)-Br(2) 113.27(2)
	Co(1)-Br(2) 2.382(6)	N(1)-Co(1)-Br(1) 109.39(7)
	Co(1)-N(1) 2.032(2)	N(1)-Co(1)-Br(2) 107.75(7)
	Co(1)-N(2) 2.059(2)	N(1)-Co(1)-N(2) 111.90(10)
		N(2)-Co(1)-Br(1) 107.98(7)
		N(2)-Co(1)-Br(2) 106.57(7)
2, $[Ni(PPh_3)_2Cl_2]$	Ni(1)-P(1) 2.366(5)	P(1)-Ni(1)-P(1) 112.00(3)
	P(1)-Ni(1) 2.366(5)	Cl(1)-Ni(1)-P(1) 104.95(2)
	Ni(1)-Cl(1) 2.202(6)	Cl(1)-Ni(1)-P(1) 103.82(2)
	Cl(1)-Ni(1) 2.202(6)	Cl(1)-Ni(1)-P(1) 103.82(2)
		Cl(1)-Ni(1)-P(1) 104.95(2)
		Cl(1)-Ni(1)-Cl(1) 127.25(4)

Important intermolecular contacts have been identified in the crystal structure of **1** (Fig. 2). These contacts (C7-H7…Br1, 3.006 Å and C1…Br2, 3.545 Å) interconnect the adjacent molecular units that create linear chains along the *a* crystallographic axis. In case of the crystal structure of **2**, no intermolecular contacts shorter than the sum of the van der Waals radii have been found.

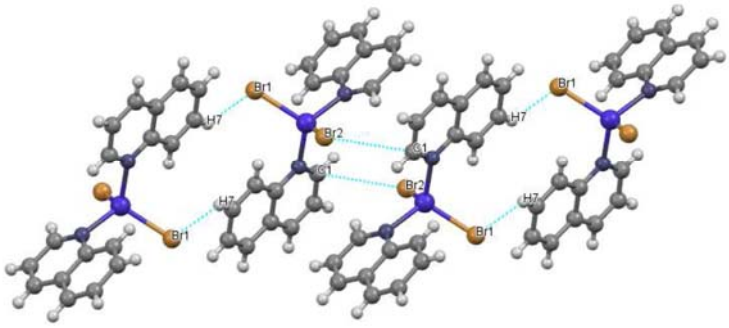

Fig. 2. Intermolecular contacts in **1**.

The solid state electronic spectra of **1** and **2** are shown in Fig. 3. For complex **1** a number of d-d transitions can be identified in the range of 9 000 – 24 000 cm^{-1} which are followed by an intense charge transfer band. The first visible transition is a broad band at ca 9 000 cm^{-1}, the second is split into three peaks between 15 000 – 17 000 cm^{-1}. Furthermore, a weak band at ca 20 000 cm^{-1} is also visible. In the spectrum of **2**, three relatively intense bands are present at ca 11 000, 18 000 and 24 000 cm^{-1}. The second band is broad and asymmetric suggesting the presence of a number of d-d transitions.

Since the structure of the complexes is derived from a tetrahedron, the interpretation of the spectra can be done in the T_d group of symmetry in the first approximation. The estimate for the crystal-field strength for tetrahedral systems is $Dq(T_d) = (4/9)Dq(O_h) = (4/9)(1/6)F_4(R)$ (BOČA, 2006).

The first transition in **1** is $^4A_2 \rightarrow {}^4T_2$ that lies in the NIR region. It has not been detected by the used hardware. The first observed band refers to the $^4A_2 \rightarrow {}^4T_1(F)$ transition and its energy is about $18Dq$ = 9 000 cm^{-1}. An estimate for the next allowed d-d transition $^4A_2 \rightarrow {}^4T_1(P)$ is $12Dq + 15B$. Using Dq = 500 cm^{-1} the Racah parameter of Co^{II} is estimated as B = 733 cm^{-1}. This value is lowered relative to the free-ion value (B_0 = 980 cm^{-1}) owing to the nephelauxetic effect (LEVER, 1984). The assignment of the individual transitions within the band in the 15 000 – 17 000 cm^{-1} region can be done in the more realistic D_{2d} group of symmetry (or C_{2v}) where the $^4T_{1g}(P)$ mother term is split into $\{^4A_2, {}^4E\}$ daughter terms. In such a case also a spin-forbidden transitions can be considered since the close-lying $^2E(G)$, $^2A_1(G)$, $^2T_1(G)$ and $^2T_2(G)$ terms might borrow the intensity from the spin-allowed transitions. The spin-orbit coupling is also in the play and it further modifies the term scheme.

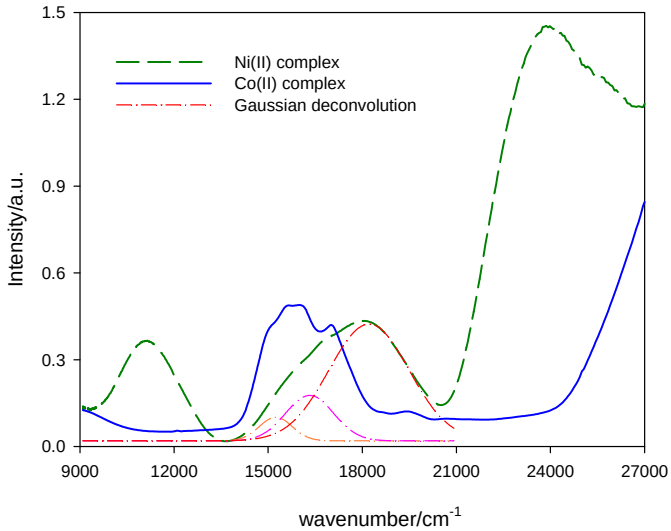

Fig. 3. Solid state electronic spectra (nujol mull) of complexes under study. Deconvolution of the second band of complex **2** using three Gaussian primitives (dot-dashed lines).

In complex **2**, we expect three principal d-d transitions considering the T_d group of symmetry. The first transition, $^3T_1 \rightarrow {}^3T_2$ (3 500 cm^{-1}), lies in the IR region (using the electronic structure parameters $10Dq$ = 3 850 cm^{-1}, B = 725 cm^{-1}). The second one appears at 6 550 cm^{-1}, $^3T_1 \rightarrow {}^3A_2$. The third transition is located in 14 250 – 15 240 cm^{-1} region, $^3T_1 \rightarrow {}^3T_1(P)$. This assignment is, however, hypothetical since the real symmetry of **2** is lower than T_d, most likely C_{2v}. Thus the $^3T_1(F,P)$ and $^3T_2$ terms are split into $\{^3A_2, {}^3B_1, {}^3B_2\}$ and $\{^3A_1, {}^3B_1, {}^3B_2\}$ terms, respectively. Furthermore, the configuration interactions between ground and excited

terms are effective causing the shift of the transitions. To elucidate the nature of detected spectral bands we have decompose the second one into Gaussian primitives. It was found that in this region three transitions are hidden (see Fig. 3). These are the transitions to $^3A_2$, $^3B_1$ and $^3B_2$ (C_{2v}) terms. According to these results, we assume that the first visible band refers to the $^3T_1 \rightarrow {}^3A_2$ (T_d) transition shifted to a higher energy. The third most intense band at ~24 000 cm^{-1} hides the charge-transfer transitions.

The molar magnetic susceptibility for **1** and **2**, corrected for the underlying diamagnetism, has been converted to the effective magnetic moment μ_{eff} that is displayed in Fig. 4.

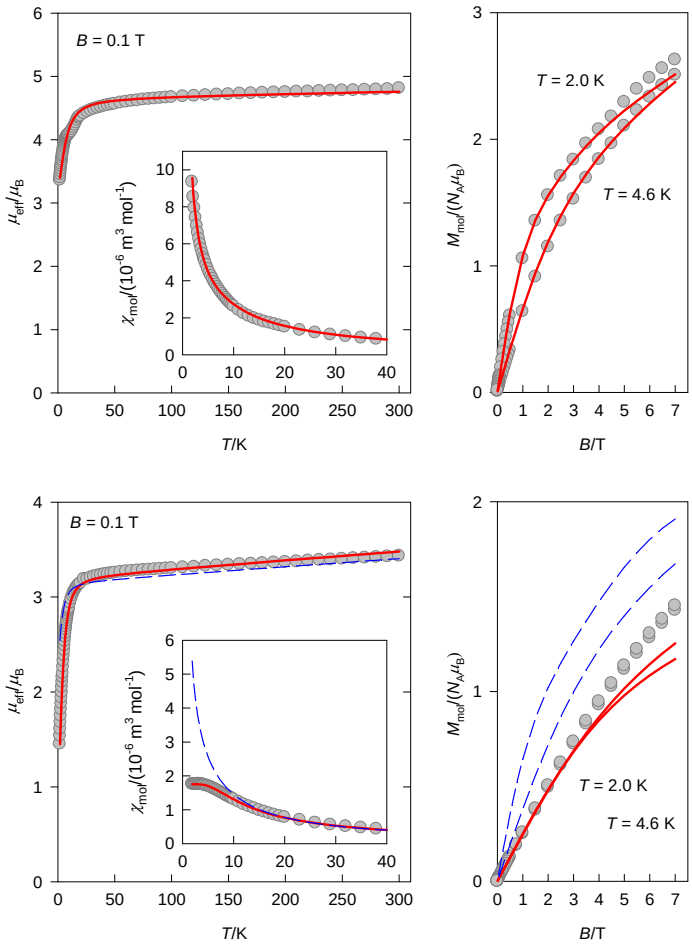

Fig. 4. Magnetic functions for complexes **1** (upper panel) and **2** (bottom panel). Left – temperature dependence of the effective magnetic moment (molar susceptibility as inset), right – field dependence of the magnetization. Circles – experimental data. Lines – fitted. Dashed lines for **2** refer to simulation with the use of negative D value ($D = -12$ cm^{-1}).

For complex **1**, at the room temperature the value of μ_{eff} = 4.85 μ_{B} matches the S = 3/2 spin system with some orbital contribution to the g-factor (g ~ 2.5). On cooling the effective magnetic moment slightly decreases along a straight line which is a fingerprint of some temperature-independent paramagnetism. Below 10 K the decrease is more rapid until 3.17 μ_{B} at 1.9 K; this reflects some zero-field splitting (the splitting of the ground $^4B_1(D_{2d})$ term into two Kramers doublets). The magnetization data taken at T = 2.0 K indicate a saturation at B > 7.0 T. The magnetization per formula unit at B = 7 T is only $M_1 = M_{\text{mol}}/(N_{\text{A}}\mu_{\text{B}})$ = 2.6 which again reflects the zero-field splitting.

Magnetic data for complex **2** are different. At the room temperature the value of μ_{eff} = 3.32 μ_{B}. This value corresponds to the S = 1 spin system with some orbital contribution. Estimated value of the g-factor is g ~ 2.3. On cooling the effective magnetic moment decreases until ~10 K, than the decrease is more rapid until 1.41 μ_{B} at 1.9 K. Here again we expect the zero-field splitting. Susceptibility data show a clear plateau at low temperatures, thus we expect positive D value in this case. With increasing field the magnetization increases rapidly. At both temperatures the behaviour is almost identical. At B = 7.0 T the magnetization per formula unit is $M_1 = M_{\text{mol}}/(N_{\text{A}}\mu_{\text{B}})$ = 1.39 and does not show a saturation feature.

The experimental magnetic data have been fitted by assuming the spin Hamiltonian in the following form:

$$\hat{H}_{k,l} = D(\hat{S}_z^2 - \vec{S}^2/3)\hbar^{-2} + E(\hat{S}_x^2 - \hat{S}_y^2)\hbar^{-2} + \mu_{\text{B}} B_m (g_x \sin\vartheta_k \cos\varphi_l \hat{S}_x + g_y \sin\vartheta_k \sin\varphi_l \hat{S}_y + g_z \cos\vartheta_k \hat{S}_z)\hbar^{-1} \quad (1)$$

where D is the axial and E is the rhombic zero-field splitting parameter, respectively. The second contribution is the spin Zeeman term. The minor improvements refer to the molecular-field correction zj and the uncompensated temperature-independent magnetism χ_{TIM}:

$$\chi_{\text{corr}} = \frac{\chi_{\text{mol}}}{1 - (zj/N_{\text{A}}\mu_0\mu_{\text{B}}^2)\chi_{\text{mol}}} + \chi_{\text{TIM}} \quad (2)$$

Table 3. Fitted magnetic parameters for complexes under study.

Compound	**1**, $[Co(qu)_2Br_2]$	**2**, $[Ni(PPh_3)_2Cl_2]$
g_x	2.643	2.284
g_y	2.544	–
g_z	2.427	2.203
D (cm^{-1})	+5.94	+12.76
E (cm^{-1})	1.24	–
χ_{TIM} (10^{-9} m^3 mol^{-1})	5.23	9.98
zj (cm^{-1})	–0.01	–
R (χ)	0.022	0.021
R (M)	0.034	0.067

An advanced fitting procedure accounts simultaneously for the two data-sets: $\chi = f(T, B_0 = 0.1\text{ T})$ and $M = f(B, T_0)$ with T_0 = 2.0 and 4.6 K, respectively. The powder

average has been done by averaging 210 points of polar coordinates (ϑ_i, φ_i) distributed over the top hemisphere. It converged to a set of magnetic parameters listed in Table 3. The quality of the fits is good as expressed by discrepancy factors for the susceptibility $R(\chi)$ and magnetization $R(M)$.

For both complexes the D value is positive. The sign of the D-parameter arises from the assignment of the lowest crystal-field multiplet. For **1**, the Kramers doublet $M_S = \pm 1/2$ is ground state and $M_S = \pm 3/2$ refers to the excited state, then $2D > 0$ holds true. In case of **2**, the ground state is the crystal-field multiplet with $M_S = 0$ and the excited one with $M_S = \pm 1$. Thus, the energy difference between these multiplets refers to $D > 0$. Positive D value has a specific effect on the progress of magnetic functions of the Ni^{II} complexes. The susceptibility of the complex **2** appears a plateau at low temperatures which is often attributed to the presence of ferromagnetic interaction between the complex molecules. In case of **2**, however, simulation of the magnetic functions (see Fig. 4) clearly confirmed that this behaviour is the result of the positive D-parameter. Also the almost identical progress of the magnetization at different temperatures is a consequence of the $M_S = 0$ ground state.

Table 4. Calculated magnetic parameters.

Compound	**1**, $[Co(qu)_2Br_2]$	**2**, $[Ni(PPh_3)_2Cl_2]$
g_1	2.222	2.243
g_2	2.275	2.339
g_3	2.284	2.379
D (cm^{-1})	+5.45	+20.06
E/D	0.03	0.17

The zero-field splitting has also been studied by *ab initio* calculations. We have applied the CAS(n,5)/NEVPT2 (n = 7 for **1**, n = 8 for **2**) methodology that results to magnetic parameters collected in Table 4. Comparing the experimental and calculated values we conclude that the correlation between them is acceptable. For complex **1** the agreement between the fitted and calculated D is excellent. However, the g-factor components are quite low, possibly due to the formation of magnetic chains in the solid state.

For complex **2** the calculated D is somewhat larger than the experimental value. Considering the earlier reported high-frequency and high-field electron paramagnetic resonance (HFEPR) spectroscopy results (D = +13.20 cm^{-1}) (KRZYSTEK *et al.*, 2002) it is evident that just the experimental D-value must be taken as the more realistic one. Overestimation of the calculated D may be associated with the omission of some important solid state effects that in such calculations cannot be included.

Contributions to the D-values that come from individual electronic transitions are presented in Fig. 5. One can see that the most important contributions are those at low transition energies (< 10 000 cm^{-1}). In complex **1**, the largest contribution (D = –14.5 cm^{-1}) comes from the transition at 4 818 cm^{-1}. This sizeable negative value is compensated by significant positive contributions mainly at 3 870 and 4 507 cm^{-1}.

In **2** the situation is analogous, however, with more pronounced *D* contributions. The *D* for the transition at 8 365 cm^{-1} is negative and very large (–48 cm^{-1}). However, the contributions from transitions at lower energies dominate at summation giving the moderate positive total *D*-value. By using this method, the origin of the positive *D*-parameter of the studied complexes can be explained.

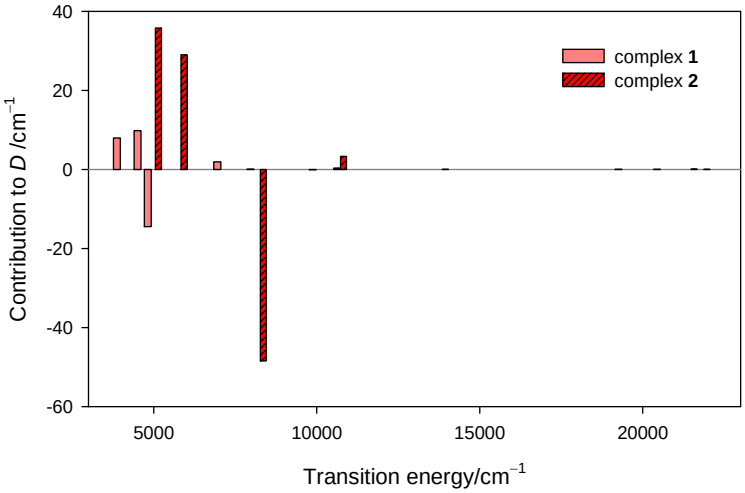

Fig. 5. Calculated contributions to the *D*-parameter from individual electronic transitions.

4. Conclusions

We have prepared two tetracoordinate complexes, namely $[Co(qu)_2Br_2]$ and $[Ni(PPh_3)_2Cl_2]$ where *qu* = quinoline and PPh3 = triphenylphosphine are N-donor and P-donor ligands, respectively. From structurally point of view these complexes are not new, since such structures are in disposal in structural database. We have redetermined the structure of these complexes and studied their spectral and magnetic properties. Static magnetism has been studied by using the DC SQUID magnetometry. We confirmed that the studied complexes exhibit a moderate magnetic anisotropy expressed by zero-field splitting parameter *D*. The *D*-value is positive for both complexes with D/hc = +5.94 cm^{-1} for the Co^{II} and D/hc = +12.76 cm^{-1} for the Ni^{II} complex. These results have been supported by *ab initio* calculations. Based on these results, we do not expect the slow magnetic relaxation for these complexes.

Acknowledgments: Slovak grant agencies (APVV-14-0078, APVV-14-0073 and VEGA 1/0534/16) are acknowledged for the financial support.

References

ALTOMARE, A., BURLA, M.C., CAMALLI, M., CASCARANO, G.L., GIACOVAZZO, C., BUAGLIARDI, A., MOLITERNI, A.G.G., POLIDORI, G.,

SPAGNA, R.: SIR97: a new tool for crystal structure determination and refinement. J. Appl. Chryst., 32, 1999, 115-119.

ANGELI, C., CIMIRAGLIA, R., EVANGELISTI, S., LEININGER, T., MALRIEU, J.P.: Introduction of n-electron valence states for multireference perturbation theory. J. Chem. Phys., 114, 2001, 10252.

ANGELI, C., CIMIRAGLIA, R., MALRIEU, J.P.: n-electron valence state perturbation theory: A spinless formulation and an efficient implementation of the strongly contracted and of the partially contracted variants. J. Chem. Phys., 117, 2002, 9138.

ANGELI, C., BORINI, S., CESTARI, M., CIMIRAGLIA, R.: A quasidegenerate formulation of the second n-electron valence state perturbation theory approach. J. Chem. Phys., 121, 2004, 4043.

ATANASOV, M., GANYUSHIN, D., PANTAZIS, D.A., SIVALINGAM K., NEESE, F.: Detailed ab initio first-principles study of the magnetic anisotropy in a family of trigonal pyramidal iron(II) pyrrolide complexes. Inorg. Chem., 50, 2011, 7460-7477.

BOČA, R.: Zero-field splitting in metal complexes. Coord. Chem. Rev., 248, 2004, 757-815.

BOČA, R.: Magnetic function beyond the Spin-Hamiltonian. *In*: MINGOS, D.M.P. (Ed.), Structure and bonding, Springer Berlin Heidelberg, 2006 1-264.

CLARK, R.C., REID, J.S.: The analytical calculation of absorption in multifaceted crystals. Acta Chryst. A, 51, 1995, 887-897.

CCDC (Cambridge Crystallographic Data Centre): http://www.ccdc.cam.ac.uk/. 2016.

FROST, J.M., HARRIMAN, K.L.M., MURUGESU, M.: The rise of 3-d single-ion magnets in molecular magnetism: towards materials from molecules. Chem. Sci., 7, 2016, 2470-2491.

GARTON, G., HENN, D.E., POWELL, H.M., VENANZI, L.M.: Tetrahedral nickel(II) complexes and the factors determining their formation. Part V. The tetrahedral co-ordination of nickel in dichlorobistriphenylphosphinenickel. J. Chem. Soc., 1963, 3625-3629.

GANYUSHIN, D., NEESE, F.J.: First-principles calculations of zero-field splitting parameters. J. Chem. Phys., 125, 2006, 24103.

GATTESCHI, D., SESSOLI, R., VILLAIN, J.: Molecular nanomagnets, Oxford University Press, 2006. 395 p.

IDEŠICOVÁ, M., TITIŠ, J., KRYZSTEK, J., BOČA, R.: Zero-field splitting in pseudotetrahedral Co(II) complexes: a magnetic, high-frequency and -field EPR, and computational study. Inorg. Chem., 52, 2013, 9409-9417.

KORCHAGIN, D.V., SHILOV, G.V., ALDOSHIN, S.M., MORGUNOV, R.B., TALANTSEV, A.D., YUREVA, E.A.: Halogen atom effect on the magnetic anisotropy of pseudotetrahedral Co(II) complexes with a quinoline ligand. Polyhedron, 102, 2015, 147-151.

KRZYSTEK, J., PARK, J.H., MARK, W., MEISEL, W.M., MICHAEL, A., HITCHMAN, A.M., STRATEMEIER, H., BRUNEL, C.L., TELSER, J.: EPR spectra from "EPR-Silent" species: High-frequency and high-field EPR

spectroscopy of pseudotetrahedral complexes of nickel(II). Inorg. Chem., 41, 2002, 4478-4487.
LEVER, A.B.P.: Innorganic electronic spectroscopy, Elsevier, New York, 1984, 863 p.
NEESE, F.: ORCA – An ab Initio, density functional and semi-empirical program package, Version 3.0.3.
NEESE, F.J.: Efficient and accurate approximations to the molecular spin-orbit coupling operator and their use in molecular g-tensor calculations. J. Chemical Physics., 122, 2005, 34107.
NEESE, F.J.: Calculation of the zero-field splitting tensor on the basis of hybrid density functional and Hartree-Fock theory. J. Chemical Physics., 127, 2007, 164112.
NEESE, F.: The ORCA program system. Rev. Comput. Mol. Sci., 2, 2012, 73-78.
OXFORD DIFFRACTION: CRYSALIS–CCD and CRYSALIS-RED, Oxford Diffraction Ltd, Abingdon, England, 2010.
SHELDRICK, M.: A short history of SHELX. Acta Chrystallogr. A, 64, 2008, 112-122.
TITIŠ, J., BOČA, R.: Magnetostructural D correlation in nickel(II) complexes: reinvestigation of the zero-field splitting. Inorg. Chem., 49, 2010, 3971-3973.
TITIŠ, J., BOČA, R.: Magnetostructural D correlations in hexacoordinated cobalt(II) complexes. Inorg. Chem., 50, 2011, 11838-11845.

Received *16 November 2016*
Accepted *5 December 2016*